GEOPHYSICS, VOL. 82, NO. 3 (MAY-JUNE 2017); P. U61–U73, 10 FIGS., 1 TABLE.
10.1190/GEO2016-0368.1

Time-average velocity estimation through surface-wave analysis: Part 2 — P-wave velocity

Laura Valentina Socco[1] and Cesare Comina[2]

ABSTRACT

Surface waves (SWs) in seismic records can be used to extract local dispersion curves (DCs) along a seismic line. These curves can be used to estimate near-surface S-wave velocity models. If the velocity models are used to compute S-wave static corrections, the required information consists of S-wave time-average velocities that define the one-way time for a given datum plan depth. However, given the wider use of P-wave reflection seismic with respect to S-wave surveys, the estimate of P-wave time-average velocity would be more useful. We therefore focus on the possibility of also extracting time-average P-wave velocity models from SW dispersion data. We start from a known 1D S-wave velocity model along the line, with its relevant DC, and we estimate a wavelength/depth relationship for SWs. We found that this relationship is sensitive to Poisson's ratio, and we develop a simple method for estimating an "apparent" Poisson's ratio profile, defined as the Poisson's ratio value that relates the time-average S-wave velocity to the time-average P-wave velocity. Hence, we transform the time-average S-wave velocity models estimated from the DCs into the time-average P-wave velocity models along the seismic line. We tested the method on synthetic and field data and found that it is possible to retrieve time-average P-wave velocity models with uncertainties mostly less than 10% in laterally varying sites and one-way traveltime for P-waves with less than 5 ms uncertainty with respect to P-wave tomography data. To our knowledge, this is the first method for reliable estimation of P-wave velocity from SW data without any a priori information or additional data.

INTRODUCTION

The present paper is the companion paper of Socco et al. (2017), which will be referred to as paper 1. In paper 1, we outline the use of surface waves (SWs) in seismic exploration records to directly estimate the S-wave time-average velocity that can be used to directly compute V_S static corrections. Several authors (Al Dulaijan and Stewart, 2010; Boiero et al., 2013; Gendrin et al., 2015) state that the use of SW for V_S static estimation is a standard method currently applied in industrial processing workflows. However, because most hydrocarbon seismic exploration data are P-wave data, the most useful information to be estimated would be V_P statics. SWs are usually considered not suitable for this purpose because it has been shown that the sensitivity of SW dispersion curves (DCs) to V_P is insufficient for a reliable V_P estimation through DC inversion. Nazarian (1984) showed that the effect of the Poisson's ratio variation, from 0.15 to 0.49, on the DC phase velocity is less than 10%. Xia et al. (1999) showed that the variability of the DC due to a variation in P-wave velocity in the model is negligible with respect to V_S and thicknesses. For this reason, in the standard procedure of SW inversion, the value of V_P (or Poisson's ratio) for the layered system is usually assumed a priori and only S-wave velocity and thickness of the layers are estimated.

Nevertheless, several attempts have been made to estimate V_P near-surface velocity models from SW DCs. In particular, the role of higher modes to improve sensitivity toward V_P has been investigated. Ernst (2008) claimed that higher modes have higher sensitivity to V_P, contrary to Xia et al. (2003), who showed that individual higher modes have lower variability than fundamental mode for V_P variations in the model. Barreto (2013) performed an extensive analysis on synthetic data to investigate the possibility of exploiting the distance between modal curves to estimate V_P, concluding that for a layered system, Poisson's ratio cannot be reliably estimated even by including higher modes. Bergamo and

First presented at the EAGE 77th Annual Conference and Exhibition. Manuscript received by the Editor 12 July 2016; revised manuscript received 2 December 2016; published online 21 March 2017.
[1]Politecnico di Torino, Torino, Italy. E-mail: valentina.socco@polito.it.
[2]Università di Torino, Torino, Italy. E-mail: cesare.comina@unito.it.

Socco (2016) showed that for very simple velocity profiles, such as gravity-induced velocity gradients with constant Poisson's ratio with depth, fundamental plus higher modes can be jointly inverted to estimate the V_S gradient and Poisson's ratio value. They applied this concept to a loose sand body and proved that P-wave velocity could be retrieved by including higher modes in SW inversion. Few authors also showed the potential of estimating V_P through the inversion of P-guided waves or SW leaky modes (Boiero et al., 2009; Ponomarenko et al., 2013; van Dedem et al., 2014); nevertheless, the presence of these kinds of guided waves is limited to a minority of data sets.

Given the weak sensitivity of SW DC to V_P, it is a common practice to estimate the Poisson's ratio value from independent data and use it to transform the V_S model obtained from SW inversion into a V_P model. Strobbia et al. (2010) showed an interesting field example in which the V_S model estimated from ground roll inversion down to a depth of 200 m was transformed into a V_P model in the first 80 m thanks to an approximated V_P/V_S ratio obtained from P-wave refraction. An alternative approach is to jointly invert SW and P-wave traveltimes from the same data set to obtain a more reliable V_S and V_P model. Boiero and Socco (2014) showed that the constraints coming from SW can significantly improve the reliability of P-wave tomograms, particularly in those environments in which highly attenuating near-surface materials can make the P-wave first-break autopicking unreliable (Badji et al., 2016).

The aforementioned works would lead us to conclude that SW cannot be used to directly estimate V_P models if other information is not available (e.g., other surveys, higher modes, or geologic information). However, there are contrasting opinions on the general sensitivity of SW to Poisson's ratio. Foti and Strobbia (2002) showed that if the a priori assumption on Poisson's ratio made during SW inversion is significantly wrong, this can affect the goodness of the estimated V_S model. They also recommended that careful analysis of a priori information should be performed to select Poisson's ratio values used in inversion because V_P and V_S properties are intrinsically related to SW propagation. Karray and Lefebvre (2008) stated that "the effect of Poisson's ratio on the construction of the theoretical dispersion relationships, associated with the inversion process, has not received enough attention and remains poorly documented." In particular, they investigated the influence of the choice of the a priori Poisson's ratio on the estimated V_S model. They used synthetic models with a constant Poisson's ratio with depth and showed that for high V_S gradient with depth, the influence of Poisson's ratio cannot be neglected. These works did not aim to estimate V_P from SWs but to warn about the need for a proper a priori choice of Poisson's ratio in the inversion performed for V_S estimation. Nevertheless, they showed that information on Poisson's ratio is potentially present in SW propagation.

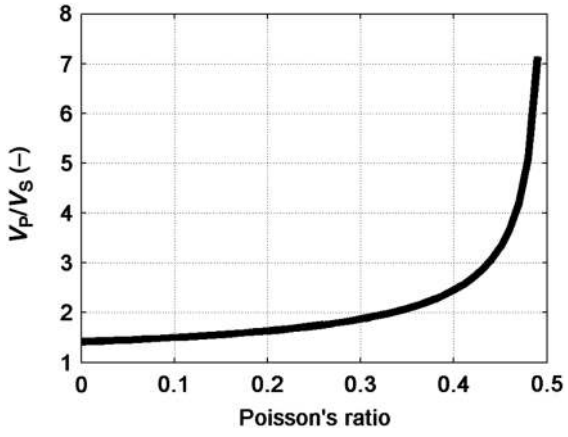

Figure 1. Poisson's ratio versus V_P/V_S (equation 2).

Some authors point out that the effect of Poisson's ratio on SW propagation is related to the investigation depth expressed as a ratio between the investigated thickness and the SW wavelength. Pelekis and Athanasopoulos (2011) proposed a simplified SW inversion technique based on the empirical estimation of an "investigation depth coefficient" that is used to directly convert the DC into an approximated V_S model. They also showed that this coefficient depends on Poisson's ratio. Pan et al. (2013) also proposed an empirical linear relationship between a penetration depth coefficient and Poisson's ratio. Although these works again did not aim to estimate Poisson's ratio or V_P, they pointed out that the sensitivity of the investigation depth to Poisson's ratio is evident and has a simple pattern.

In paper 1, we exploited the concept of penetration depth of SW for a simplified time-average V_S model estimation. Our approach was based on the estimation of a piecewise polynomial relationship between the wavelength and the depth (W/D). In this paper, we investigate the sensitivity of the W/D relationship to Poisson's ratio and show that this sensitivity can be used to estimate Poisson's ratio to transform the time-average V_S model into a time-average V_P model. The time-average velocity, consistently with paper 1, is defined as:

$$V_z = \frac{\sum_n h_i}{\sum_n \frac{h_i}{V_i}}, \tag{1}$$

where n is the number of layers down to the depth z, and h_i and V_i are the thickness and the velocity of the ith layer, respectively. This velocity provides directly the one-way time at a selected depth z. The proposed approach is already introduced by Socco et al. (2016) and applied to a synthetic data set. Here, we describe the method in detail and justify its validity. We then test it on two field data sets.

Because we will estimate Poisson's ratio to transform the time average S-wave velocity V_{Sz} into the time average P-wave velocity V_{Pz}, it is useful to examine the expected values of Poisson's ratio in near-surface materials and how accurate its estimate should be to provide a reliable V_{Pz}. Moreover, it is also important to address the expected spatial variability of Poisson's ratio in near-surface layers.

First, it should be stressed that when we relate Poisson's ratio to seismic velocities, we are implicitly assuming to deal with the so-called dynamic Poisson's ratio, i.e., Poisson's ratio at small strain level and in undrained conditions. The dynamic Poisson's ratio ν (in the following Poisson's ratio) is related to seismic velocities as shown in equation 2:

$$\nu = \frac{1}{2}\frac{\left(\frac{V_P}{V_S}\right)^2 - 2}{\left(\frac{V_P}{V_S}\right)^2 - 1}, \tag{2}$$

where V_P and V_S are the P- and S-wave velocities, respectively. Hence, Poisson's ratio is a nonlinear scaling factor between V_P and V_S. By plotting equation 2, we can see (Figure 1) that the sensitivity of V_P/V_S to Poisson's ratio varies for different ranges of Poisson's ratio value. In particular, at Poisson's ratio values less than 0.4, the V_P/V_S varies from 1.4 to 2.5 and small variations in Poisson's ratio will induce very small variations in V_P/V_S. Hence, for materials in this range of Poisson's ratio, if V_S is available and Poisson's is estimated and used to retrieve V_P, an error of 0.01 in Poisson's ratio estimation will cause an error from 0.5% to 3.9% on V_P, whereas an error of 0.1 on Poisson's ratio will cause an error from 6% to 24% on V_P. Conversely, in the range above 0.4, the error grows up to almost 50% for a Poisson's ratio of 0.48 and reaches almost 100% for a Poisson's ratio equal to 0.499.

Hence, in different ranges of Poisson's ratio, different accuracies are required. In the literature, there are relatively few data collections of Poisson's ratio values. One of the largest to our knowledge is a series of seismic borehole measurements performed by the USGS over decades and reported by Boore (2007). The available data from 274 downhole tests and 53 suspension logging tests show that in saturated soils, Poisson's ratio is strongly governed by saturating fluids and assumes poorly dispersed values, which are very close to 0.5. In the case of dry soils or weathered rocks, the values appear to be more variable with the majority of field data in the range of 0.25–0.4. Along the vertical direction, abrupt variations in Poisson's ratio can be encountered at the water table and at the bedrock interfaces. Even though at the water table the variation is mainly due to a variation in V_P with almost unchanged V_S, at the bedrock, both V_P and V_S change. Along the lateral direction, abrupt variations in Poisson's ratio are generally related to sharp variations in the solid matrix properties. Thus, the variations will concern both V_P and V_S. This is an important point for the method we propose because we estimate one Poisson's ratio vertical profile in correspondence with one reference DC and we use it to convert the V_{Sz} estimated along the line into V_{Pz}. Hence, we make the assumption that lateral variations in Poisson's ratio are expected to be negligible along the line. We also assume that if a significant lateral variation in Poisson's ratio is present along the line, this will correspond to a significant variation in V_S that will show up in the experimental DCs. In this case, the data set can be split into subdata sets and a reference Poisson's ratio profile can be estimated for each of them.

This paper is organized as follows: First, we outline the method using a single synthetic 1D model example with the constant Poisson's ratio with depth, and then, we test the method on more challenging synthetic profiles with a variable Poisson's ratio with depth and also in the presence of a low-velocity layer. We finally apply the method to the same field data shown in paper 1, and we compare the estimated V_{Pz} models with those obtained through traveltime tomography and local downhole tests.

METHOD

In paper 1, we have introduced the W/D relationship that can be used to directly estimate the time average S-wave velocity (V_{Sz}) given the SW DC. As for paper 1, in this work, we refer to fundamental mode only; hence, for "dispersion curve," we intend "dispersion curve of the fundamental mode of propagation of Rayleigh waves." Here, we show that the W/D relationship is sensitive to Poisson's ratio and can therefore also be used to estimate the time average P-wave velocity V_{Pz}. We use the same synthetic V_S model used in paper 1 to outline the method. We start by assuming a constant Poisson's ratio of 0.33 for all of the layers. In Figure 2a, we report the V_P and V_S models, the resulting V_{Pz} and V_{Sz}, and the relevant fundamental mode DC plotted as a function of wavelength. From the time-average V_S model and the DC, we compute the W/D relationship by searching, for each V_{Sz} value, the wavelength at which the phase velocity of the DC is equal to V_{Sz}. We take the V_{Pz} model and the W/D relationship as our reference (we call them "experimental" data), and we show that the W/D relationship can be used to estimate V_{Pz}.

We then keep the V_S model as it is and change the Poisson's ratio for the whole model, ranging from 0.1 to 0.45, and we compute the theoretical DCs corresponding to different values of Poisson's ratio. We use these DCs and the V_{Sz} to compute the W/D relationships for the different values of Poisson's ratio. In Figure 2b, we report all the obtained W/D relationships together with the one of the reference V_P model in Figure 2a. It can be noted that Poisson's ratio acts on the slope of W/D relationship. In particular, the slope decreases when Poisson's ratio increases.

By comparing the experimental W/D relationship with the theoretical ones, we can identify the Poisson's ratio value that matches the experimental data. The comparison is performed, similarly to Socco et al. (2016), by associating to each depth the value of Poisson's ratio that corresponds to the linear interpolation between the values of ν_z^+ and ν_z^-, where ν_z^+ and ν_z^- are the values at the upper and lower nearest constant Poisson's ratio W/D relationship, respec-

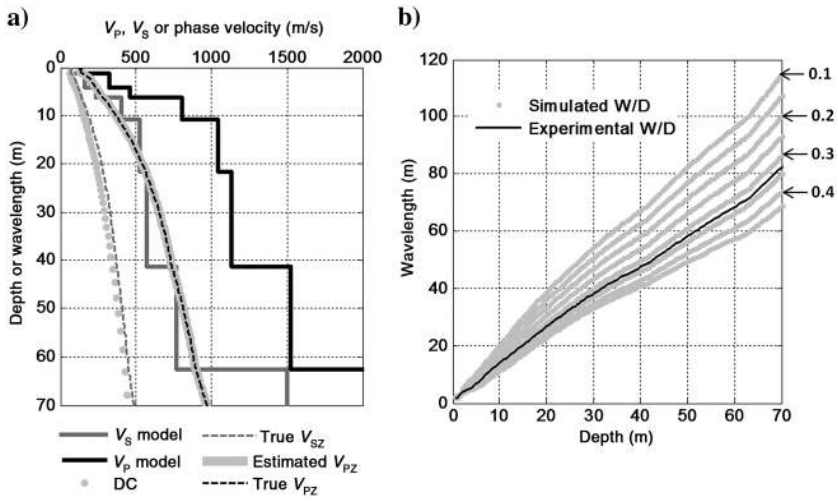

Figure 2. (a) The synthetic V_P and V_S model (black and gray solid), the corresponding V_{Pz} and V_{Sz} (black and gray dashed line), the estimated V_{Pz} (gray solid), and Rayleigh wave DC as a function of wavelength (gray dots). The vertical axis corresponds to z for the velocity models and to wavelength for the DC; the horizontal axis corresponds to V_S and V_P for the velocity models and to the Rayleigh wave phase velocity for the DC. (b) The W/D relationship for the reference model of plot (a) (black) compared with the ones obtained with different Poisson's ratio values (gray). Some reference Poisson's ratio values are indicated on the right of the plot.

tively. Then, we use the estimated Poisson's ratio ν_z to calculate the V_{Pz} starting from the V_{Sz} using equation 3:

$$V_{Pz} = V_{Sz}\sqrt{\frac{2(\nu_z - 1)}{2\nu_z - 1}}. \quad (3)$$

We compare the estimated and true V_{Pz} models in Figure 2a. In this case, the retrieved Poisson's ratio has a constant value with depth that corresponds to the true value, and hence, the estimated and true V_{Pz} are exactly coincident.

In Figure 2, we have shown that the W/D relationship is sufficiently sensitive to Poisson's ratio to identify the true Poisson's ratio and estimate V_{Pz}. This sensitivity is the result of the link between Poisson's ratio and the investigation depth. This can be shown by considering the Rayleigh wave vertical displacement pattern with depth. In Figure 3a, we show the normalized vertical displacements of the fundamental mode of Rayleigh wave propagation computed for the reference V_S model and different values of Poisson's ratio, for a frequency equal to 6 Hz. The vertical displacements are computed using the code implemented by Maraschini (2008) and based on the work of Herrmann (2002) who uses the method introduced by Thomson (1950) and Haskell (1953) and modified by Dunkin (1965). It can be seen that the propagation spans different depths, and for a higher Poisson's ratio, the investigation depth is higher.

The link between W/D relationship slope and Poisson's ratio is shown by plotting the normalized amplitude of vertical displacements at different depths for each propagating wavelength. This is shown in Figure 3b–3f for the V_S reference model in Figure 2a and different constant values of Poisson's ratio. As already shown in paper 1, the W/D relationships roughly fall within the zone where the amplitude of the displacements becomes negligible (approximately 10%). Here, we observe that this boundary clearly changes according to Poisson's ratios and that the slope decreases when Poisson's ratio increases.

Thus far, we have used a simple example with a constant Poisson's ratio value for the whole model to show the sensitivity of the W/D relationship toward Poisson's ratio. In the following, we present three examples of 1D models with variable Poisson's ratio with depth and growing complexity. The first two models are in the range of Poisson's ratio values typical of dry sediments or soft rocks: Poisson's ratio is equal to 0.33 in the first four layers and

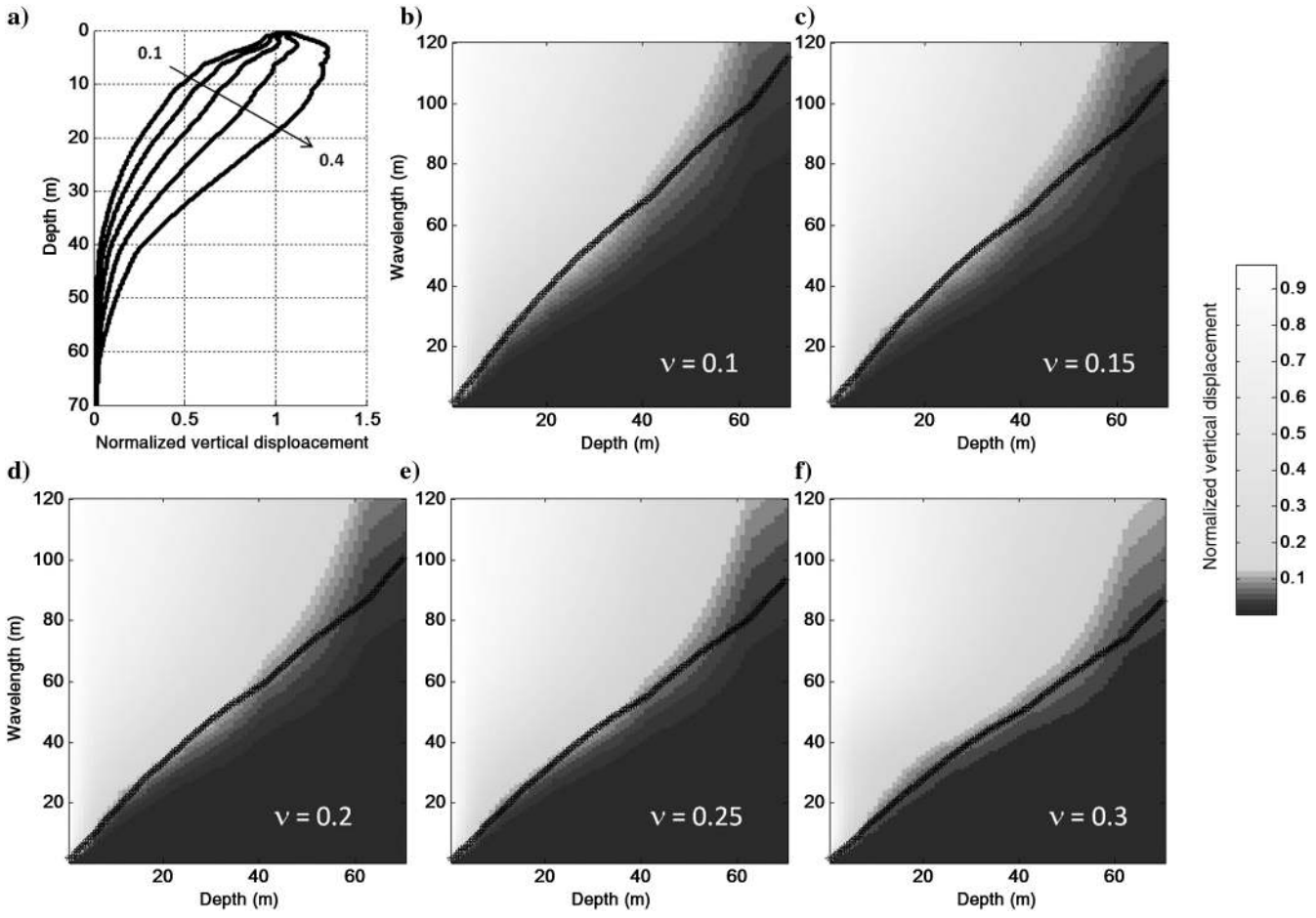

Figure 3. (a) Vertical displacement for the fundamental mode of Rayleigh wave normalized with respect to the displacement at $z = 0$ for the V_S model in Figure 2a and different values of Poisson's ratio for the frequency 6 Hz . (b-f) Normalized amplitude of vertical displacements at different depths for each propagating wavelength for the same V_S model and different values of Poisson's ratio with the corresponding W/D relationship (black lines).

is equal to 0.2 for the deeper layers. In the first model V_S always grows with depth, while in the second model there is a velocity inversion at the interface corresponding to Poisson's ratio change. The third synthetic model is more challenging and has Poisson's ratio varying in each layer ranging from 0.2 to 0.45. In Figure 4, we report the results of our analyses for the three models. In Figure 4a–4c, we show the V_P models with the corresponding V_{PZ} and the relevant DC plotted as a function of wavelength.

In Figure 4d–4f, we report the experimental W/D relationship of each reference model, compared with the W/D relationships computed with constant Poisson's ratios. We estimate Poisson's ratio with depth as explained above. The estimated ν_z for the different

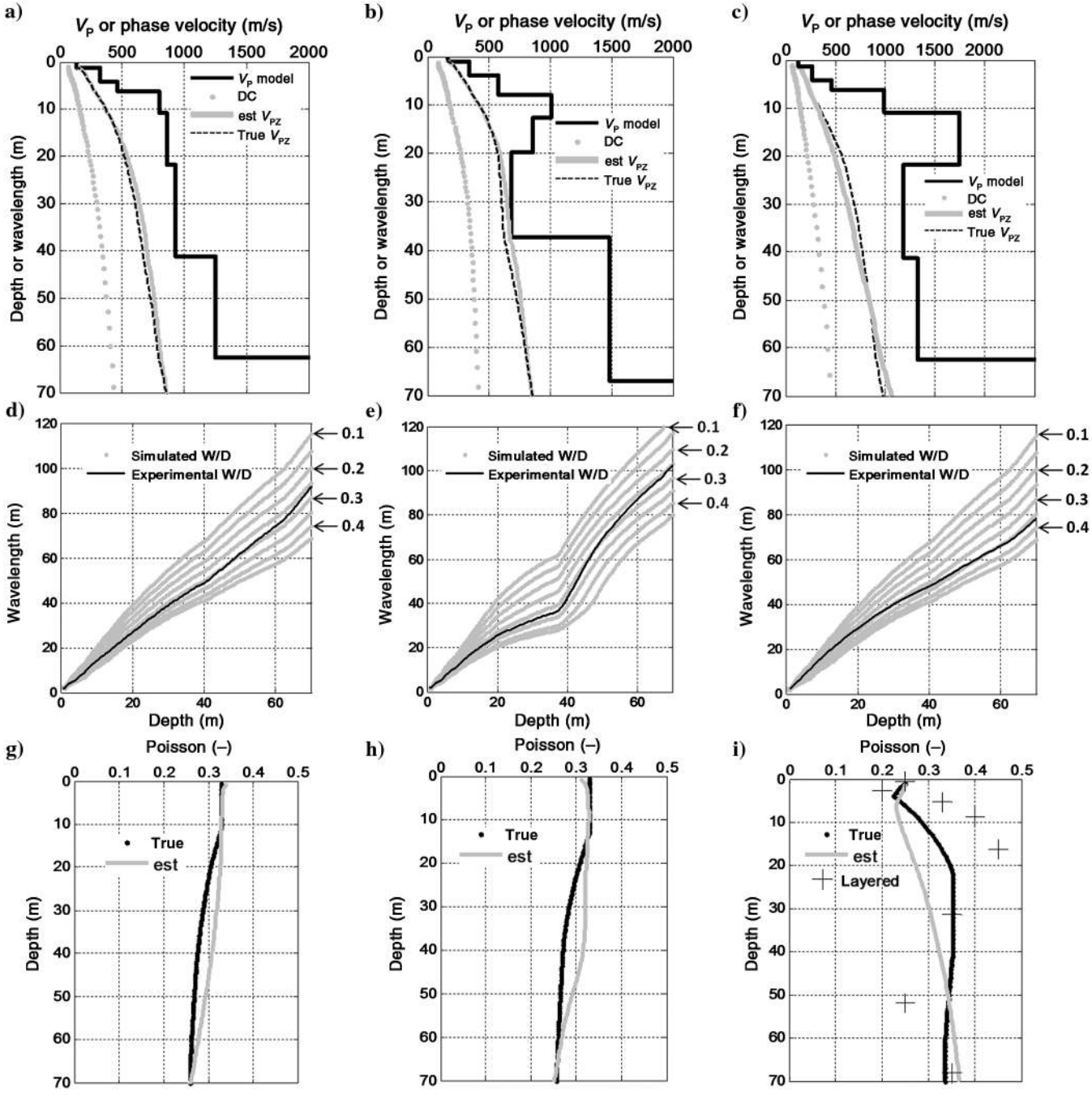

Figure 4. Synthetic examples with variable Poisson's ratio with depth: (a-c) The synthetic V_P models (black solid), the corresponding true V_{PZ} (black dashed line), the estimated V_{PZ} (gray solid), and Rayleigh wave DC as a function of wavelength (gray dots), the vertical axis corresponds to z for the velocity models and to wavelength for the DC; the horizontal axis corresponds to V_P for the velocity models and to the Rayleigh wave phase velocity for the DC. (d-f) The W/D relationships for the reference models (black) compared with the ones obtained with different Poisson's ratio values (gray); some reference Poisson's ratio values are indicated on the right of the plots. (g–i) The estimated (gray) and true (black) apparent Poisson's ratios; for the example in plot (i), Poisson's ratio values of each layer are also reported.

models are reported in Figure 4g, 4h, and 4i and compared with the Poisson's ratio profile obtained from true V_{Sz} and V_{Pz} values at each depth using equation 4:

$$\nu_z = \frac{1}{2}\frac{\left(\frac{V_{Pz}}{V_{Sz}}\right)^2 - 2}{\left(\frac{V_{Pz}}{V_{Sz}}\right)^2 - 1}. \quad (4)$$

We call this ν_z the "apparent" Poisson's ratio. Equation 4 is the same as equation 2, where V_P and V_S are substituted with the time average V_{Pz} and V_{Sz}. The estimated apparent Poisson's ratios are finally used to transform the V_{Sz} profile into V_{Pz} using equation 3 and compared with the true V_{Pz} (Figure 4a-4c).

It is worth noting that for the first two examples, the true apparent Poisson's ratio corresponds with the layered Poisson's ratio in the upper part of the profile in which Poisson's ratio is constant, and then, it tends to the new value without reaching it in the considered investigation depth. Therefore, an abrupt change in the Poisson's ratio of the layered model corresponds to a smooth variation in the apparent Poisson's ratio. In these two synthetic examples, the estimated Poisson's ratio correctly retrieves the value in the uppermost portion of the model and then also tends to the lower value in the deeper portion. Nevertheless, the transition between the two apparent Poisson's ratio values is slightly oversmoothed. This effect is stronger in the second model that presents the velocity inversion. For the third example, again, the sharp variation in the layered Poisson's ratio corresponds to a smooth transition of apparent Poisson's ratio (Figure 4i); it can also be observed that in this situation, the estimated apparent Poisson's ratio shows a reduced capability of evidencing this transition.

Table 1. Absolute normalized estimation error of V_{Pz} for three models in Figure 4.

Absolute normalized errors on VPz	Synthetic case 1	Synthetic case 2	Synthetic case 3
Mean	3.46%	3.16%	3.77%
Max	6.13%	8.39%	13.75%

In spite that the estimated Poisson's ratio is smoother than the true apparent Poisson's ratio, the resulting errors in the V_{Pz} are small. In Table 1, we report the values of the estimation error on the velocity for the three synthetic cases. The greatest error is found at 20 m of depth for the profile of the third case, for which the average error is less than 4%.

We have shown that using the W/D relationship in the case of a constant Poisson's ratio with depth, it is possible to recover it and to provide a very accurate estimate of V_{Pz}. In the case of a variable Poisson's ratio with depth, we have introduced the concept of "apparent" Poisson's ratio and we have shown that the Poisson's ratio variability can be recovered from the W/D relationship. Nevertheless, with the proposed approach, the estimate shows uncertainty in the transition zone that produces low errors in the V_{Pz}. This method is, to our knowledge, the first presented method that is able to estimate the V_{Pz} of a 1D profile from SW data with this level of accuracy.

In paper 1, we showed that the W/D relationship estimated for one known V_S model and the corresponding DC can be applied to a set of DCs extracted along a seismic line to directly estimate the V_{Sz} for the whole data set. We also showed that this method is able to reconstruct the V_S lateral variability at the site. Here, we have shown that the same W/D relationship is sensitive to Poisson's ratio variability with depth and can be used to obtain an apparent Poisson's ratio profile that allows the V_{Sz} model to be converted into a V_{Pz} model. In Socco et al. (2016), we have extended this approach to estimate V_{Pz} models along the whole seismic line starting from the estimated V_{Sz} models and the estimated apparent Poisson's ratio for the reference profile. Using a synthetic data set, we have shown that the V_{Pz} of all the profiles could be recovered. Nevertheless, in those synthetic models, the Poisson's ratio was chosen to be laterally constant within each layer. We think that this assumption can be transferred to the real word with some care. As we stated in the "Introduction" section, it is reasonable to expect a stronger variability of Poisson's ratio along the vertical direction than along the horizontal direction. In particular, we expect that if a significant lateral variation in Poisson's ratio occurs, this is likely to correspond to a variation in both V_P and V_S and will therefore show up in the DC trend along the line. In this case, we can split the data set into subdata sets in which we assume negligible lateral variations in the Poisson's ratio and we estimate the Poisson's ratio for each of them. It is worth noting that when Poisson's ratio is expected to vary significantly, the method could also be applied to each individual DC curve along the line. In the following, we apply the method to the two field data sets used in paper 1. The first is processed assuming negligible lateral variations in the Poisson's ratio, and through the second field case we address the lateral variability of Poisson's ratio.

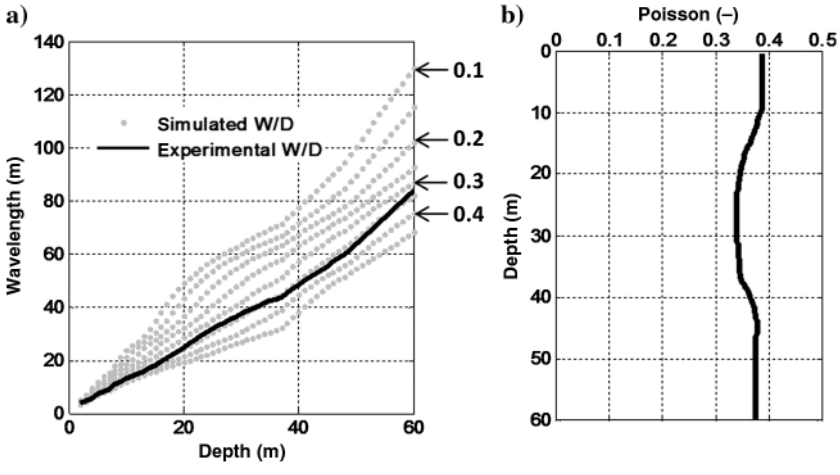

Figure 5. Field case 1: (a) the W/D relationship for the reference model (black) and those obtained for constant Poisson's ratio values using the same V_S model (gray), some reference Poisson's ratio values are indicated on the right of the plot and (b) estimated apparent Poisson's ratio for the reference model.

FIELD CASES

The two data sets are the same used in paper 1. For a brief description of their geological setting

and of the SW data, please refer to paper 1 and the references therein. We here focus on the P-wave data and on the estimation of the apparent Poisson's ratio for the reference profiles. Then, we use it to transform the V_{Sz} models along the line into V_{Pz} models. We compare the V_{Pz} estimated only by the use of SWs to benchmark results obtained on the two data sets using P-wave traveltime tomography and P-wave downhole tests. As stated in paper 1, where we compared our results with those obtained through DC inversion, we are conscious that P-wave tomography results cannot be considered as the ground truth. Nevertheless, P-wave tomography is an accepted method for near-surface P-wave velocity estimation, and being a 2D approach based on P-wave data, we think that showing that our method is able to replicate tomography results is a significant validation. Moreover, for the two field cases, the dense receiver and source layout provided a very large amount of traveltime data and the maximum offset (approximately 500 m) guaranteed a very high coverage (thousands of rays/cell) within the depth of interest for the present work (see details in Socco et al., 2008). We hence assume that the tomograms can be used as a reliable benchmark.

Field 1: La Salle

The site is located in the Alps, on the alluvial fan of La Salle (Northwest Italy). The deposit was the object of a geophysics campaign in 2007, and details about the site and DC data can be found in paper 1 and in Socco et al. (2008). The P-wave traveltimes were picked from two orthogonal high-resolution P-wave seismic reflection lines and were used to estimate near-surface V_P models using a commercial traveltime tomography code (see Socco et al. [2008] for details). Here, we focus on the DCs and P-wave tomogram along line 1. As already specified in paper 1, the DC data set has a quite good quality with a dense set of 60 smooth and continuous DCs along the line. The trend of the DCs along the line did not evidence significant variations. We used the same reference model and W/D relationship used in paper 1, which is not part of the data set, but had been obtained through Monte Carlo inversion of one of the broadband DCs obtained from the merging of SW active and passive data (located at site A in Socco et al., 2008). For the inversion of the reference DC, we used a Monte Carlo inversion algorithm (Socco and Boiero, 2008) in which model parameters are randomly sampled from uniform distributions. Usually, only V_S and layer thickness are free to vary whereas the density and Poisson's ratio are fixed a priori. Here, instead, we defined a wide model space also for Poisson's ratio with boundaries from 0.2 to 0.49 for each layer. This was done to avoid that Poisson's ratio of the reference V_S model could be biased by the a priori assumption of a fixed Poisson's ratio. In the Monte Carlo results (not shown), as expected, the sensitivity to V_S strongly prevails and the accepted models have a very narrow V_S range. On the contrary, Poisson's ratio cannot be identified from the accepted models because the obtained values span the whole model space range.

In Figure 5a, we compare the W/D relationship obtained for the reference model with the W/D relationship obtained by simulating DCs for the reference V_S model at constant Poisson's ratio values. The W/D relationship was used in paper 1 to directly transform all the DCs along the line into V_{Sz} models. Here, we have used the same W/D relationship to estimate the apparent Poisson's ratio for the reference model and we have applied it to transform all the V_{Sz} models along the line into V_{Pz} models. We have, therefore, assumed

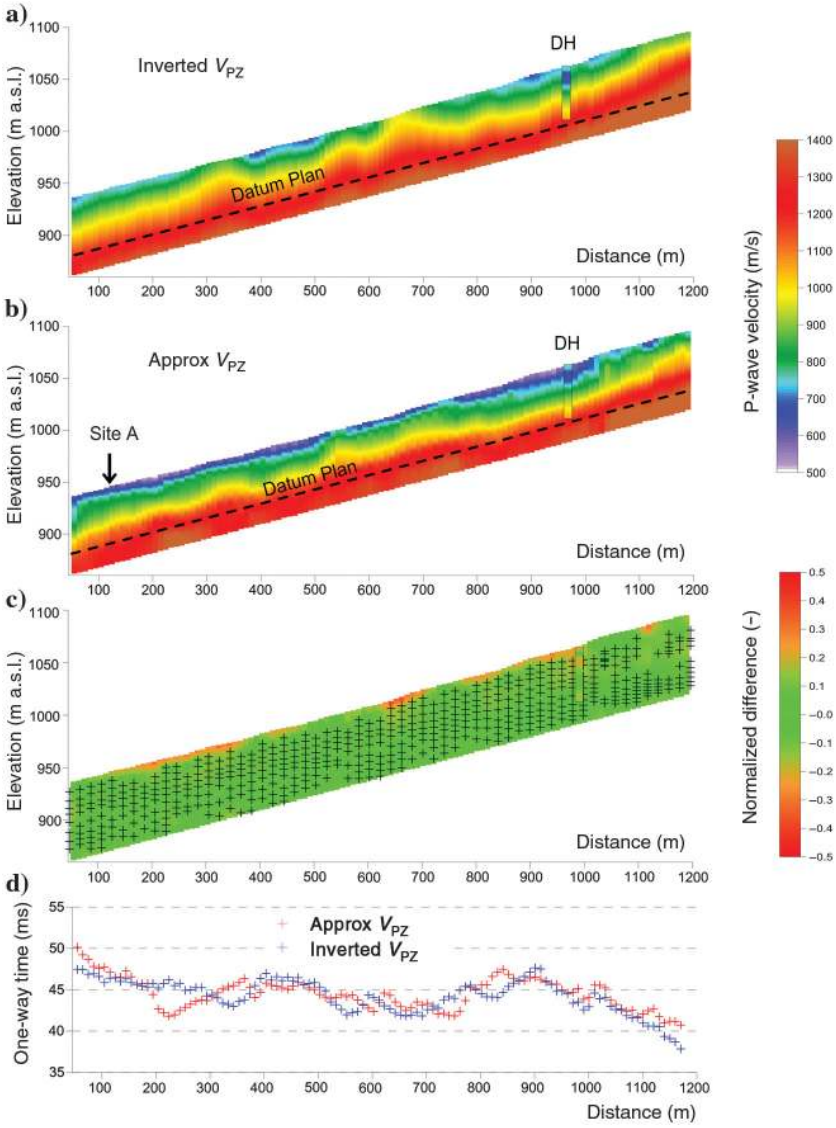

Figure 6. Field case 1: (a) V_{Pz} obtained from P-wave traveltime tomography and DHT results, (b) V_{Pz} obtained using the estimated apparent Poisson's ratio and the V_{Sz} estimated in paper 1 and DHT results, the location of the reference model (site A) is indicated by the arrow. (c) Normalized difference between the two V_{Pz} models and DH results. The black crosses represent the DC data points of all the DCs plotted as a function of wavelength. Please notice that here the normalized difference range is higher than in paper 1. d) One-way time along the line for datum plan depth reported in panels (a and b) for tomographic and approximated V_{Pz}.

that the lateral variation in Poisson's ratio was negligible along the line. In Figure 5b, we show the estimated apparent Poisson's ratio for the reference model.

We show the results in terms of V_{Pz} along the line in Figure 6 compared with the V_{Pz} models obtained by transforming the V_P model from P-wave traveltime tomography into a time-average V_{Pz}. We show the normalized difference between the two results, and consistently with paper 1, we superimpose to the difference plot the data points of the experimental DCs as a function of wavelength. We also report the results of the local downhole tests (DHT) in terms of V_{Pz} using the same color scale used for the velocity sections and the normalized difference of our results with respect to the DHT. In Figure 6d, we compare the one-way time (static shift) at a floating datum at 55 m depth along the line computed using the tomography results and our results.

The difference along the 2D section is within 10% for most of the estimated values. There are some higher difference values at very shallow depths in which the DC data points have no coverage. The slight lateral variability is properly reconstructed as already pointed out in paper 1 for V_{Sz}. Our results are also in better agreement with the DHT with respect to tomography data. The static shifts computed at a depth of 55 m (below the top of the first high-velocity layer) show maximum difference of the order of 5 ms and provide very similar trends. This field case shows that for good-quality data and smoothly laterally varying sites, the proposed direct estimation of P-wave time-average velocity can be conveniently applied.

Field 2: Torre Pellice

The site is located in an alpine valley in the town of Torre Pellice (northwest of Italy). The deposit was the object of a geophysics campaign in 2007, and details about the site, data acquisition and processing can be found in paper 1, in Socco et al. (2009), and in Boiero and Socco (2014). In this case, the benchmark is a tomographic P-wave velocity model that was obtained through a joint inversion with DCs by Boiero and Socco (2014). On this site, there is a significant lateral variability because the seismic line crosses two different geologic environments: the zone close to the river (approximately from 0 to 250 m) in the south and the zone over an alluvial fan in the north (from 320 m to the end of the line). Consistently with paper 1, we used two reference models: one from the north zone and one from the south zone, and we estimated two W/D relationships to be applied in the two zones. As specified in paper 1, for this data set, the data quality is critical: The DCs are discontinuous and noisy, with gaps in significant frequency bands. The reference DCs have been chosen as a compromise among frequency band, smoothness, continuity, and representativeness.

We performed the same analysis shown for field case 1. The W/D relationships for the reference models were estimated in paper 1. The reference DC curves were chosen among the data set, and the reference models were the corresponding V_S models obtained through the joint inversion (Boiero and Socco, 2014). The W/D relationships of these models were used in paper 1 to directly transform the DCs of the two zones along the line into V_{Sz} models.

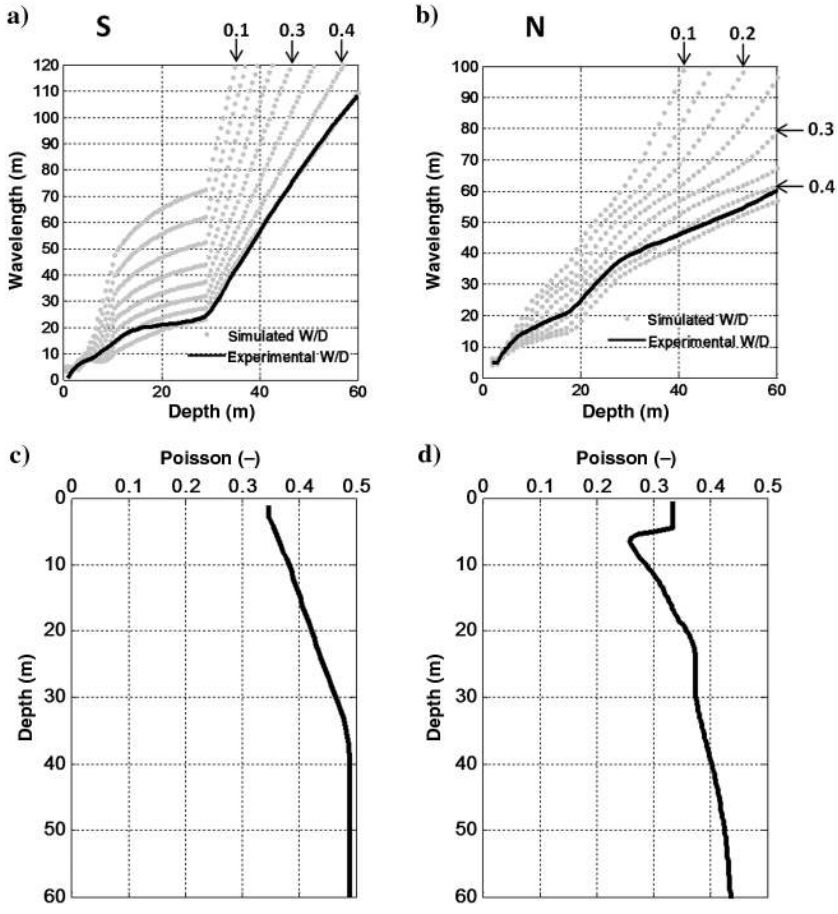

Figure 7. Field case 2: (a and b) The W/D relationships for the reference models (black) and those obtained for constant Poisson's ratio values using the same V_S model (gray). some reference Poisson's ratio values are indicated on the plots. (c and d) Estimated apparent Poisson's ratio for the reference models.

In Figure 7a and 7b, we compare the W/D relationships obtained for the reference models with the W/D relationships obtained by simulating DCs for the reference V_S models at constant Poisson's ratio values. We used the W/D relationships to estimate the apparent Poisson's ratio for the reference models, and we applied them to transform all the V_{Sz} models along the line into V_{Pz} models. We show the estimated apparent Poisson's ratios for the reference models in Figure 7c and 7d. The patterns of the apparent Poisson's ratio with depth in the two zones are different: In the south, the apparent Poisson' ratio reaches very high values at shallow depths, whereas in the north, the apparent Poisson's ratio assumes lower values. For the north zone, an abrupt variation in the estimated apparent Poisson's ratio at shallow depths can be observed. This can be related to the frequency gap contained in the reference DC (see Figure 10 in Socco et al., 2017).

We show the results in terms of V_{Pz} along the line in Figure 8 compared with the V_{Pz} models obtained from P-wave tomography. We show the normalized difference between the two results in Figure 8c, and, consistent with paper 1, we superimpose the data points of the experimental DCs as a function of wavelength. Also in this case, we report the DHT results and compare them with the tomography and our results.

The poor data coverage of the DC points has a significant impact on the quality of the final result that presents some zones of high difference with respect to benchmark. The very high difference of the profile at 320 m can be related to an anomaly in the joint inversion results. The differences with respect to the DHT results are small (mostly less than 10%) in the north zone, whereas they show a similar trend of joint inversion data in the south zone. In Figure 8d, we show the one-way time along the line for the datum plan indicated in Figure 8a and 8b (located at a depth of approximately 45 m in the north zone and 30 m in the south zone) computed from joint-inversion results and our direct estimation results. Also in this case, the trends are in good agreement and the difference is mostly within 5 ms. However, a few zones with higher differences can be observed. In Figure 8d, we also report the DHT traveltimes at datum plan depth; in the north zone, the DHT traveltime is in between our estimation and joint-inversion data.

DISCUSSION

We have proposed a new method to estimate the time average V_P (V_{Pz}) from SW dispersion data along a seismic line. The method relies on the knowledge of one V_S model that is used, together with its corresponding DC, to estimate the experimental W/D relationship. The W/D relationship is then used to estimate the apparent Poisson's ratio with depth by comparison with theoretical W/Ds for the same reference V_S model at different Poisson's ratio values. The same W/D relationship was used in paper 1 to estimate the V_{Sz} along the line and, by using the estimated apparent Poisson's ratio, the V_{Sz} is transformed here into a V_{Pz} model. The V_{Pz} can then be used to directly compute the one-way time at the desired datum plan depth within the investigation limit.

Using 1D synthetic models, we showed that, if Poisson's ratio is constant with depth, the Poisson's ratio value retrieved with this method is the correct one. In the case of a Poisson's ratio that varies with depth, we have introduced the apparent Poisson's ratio concept that relates, at each depth, the V_{Sz} and the V_{Pz}. The Poisson's ratio estimated using the W/D relationship and the true apparent Poisson's ratio show a smooth variability. Furthermore, the V_{Pz} value estimated has maximum errors less than 15% with respect to the true one, even in challenging situations. As the depth increases,

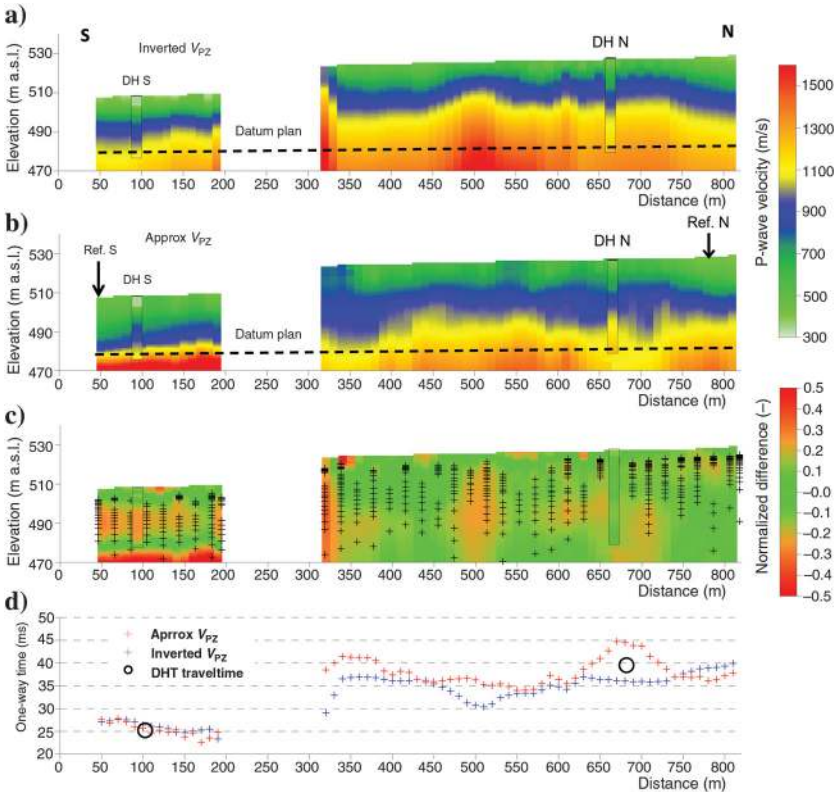

Figure 8. Field case 2: (a) V_{Pz} obtained from P-wave traveltime tomography and DHT results; (b) V_{Pz} estimated using the estimated apparent Poisson's ratio and the V_{Sz} estimated in paper 1, and location of the reference models are also evidenced together with DHT results. (c) Normalized difference between the two V_{Pz} models and DHT results. The black crosses represent the DC data points of all the DCs plotted as a function of wavelength. Please notice that the range of error values is higher than for paper 1. (d) One-way time along the line for datum plan depth reported in panels (a and b) for inverted and approximated V_{Pz} and DHT traveltimes.

the reciprocal distance among the W/D relationships at a constant Poisson's ratio increases as well. This means that the sensitivity to Poisson's ratio increases with depth (see for instance Figures 2b, 4d, 4e, and 4f), and hence the estimation improves at greater depths. In particular, the synthetic examples show that the estimation of V_{Pz} becomes very accurate below the bedrock: For the first two synthetic models, the error of the estimated P-wave one-way time at 70 m is 0.15 and 0.44 ms, respectively, whereas for the more challenging third model, it is 5.5 ms (still near the time sampling for seismic exploration data). The synthetic 1D cases have evidenced that our direct estimation tends to oversmooth the apparent Poisson's ratio profile with respect to the true profile and that this effect is more significant for large contrasts of Poisson's ratio among layers (such as in the third synthetic case in which Poisson's ratio varies between 0.2 and 0.45). Nevertheless, the corresponding errors in the obtained V_{Pz} are low (see Figure 4 and Table 1). The synthetic models used have been defined according to typical Poisson's ratio values of near-surface materials reported in the literature. Nevertheless, the strong contrasts of our synthetic models are not very common according to our experience. In particular, in dry loose granular materials (such as in sand dunes), the value of Poisson's ratio can easily be almost constant with depth and can assume typically values in the range 0.2–0.3 (Bachrach et al., 2000; Zimmer et al., 2007). Hence, even the simple example reported in Figure 2, that concerns a velocity profile with constant Poisson's ratio with depth, can be significant. As we stated in the "Introduction" section, the required accuracy in the estimate of Poisson's ratio increases for a higher value of Poisson's ratio, hence in saturated media. For this case, it is interesting to analyze the pattern of Poisson's ratio for the reference model in the south zone of field case 2, in which the W/D relationship below the water table tends rapidly to a value of almost 0.5. In this situation, even a slight overestimation of Poisson's ratio can lead to large errors in the V_{Pz}. Hence, caution is required in the application of the proposed method in these situations.

Considering the application to individual velocity profiles, it is important to specify that the proposed approach is a very simple method to exploit the sensitivity of the W/D relationship to Poisson's ratio. Other, more sophisticated methods than the proposed interpolation (for instance inversion) could be implemented to improve the accuracy of the apparent Poisson's ratio estimate for the cases in which there are strong Poisson's ratio contrasts with depth. Nevertheless, to our knowledge, this is the very first method described in the literature to directly estimate the P-wave velocity from SW DC without any additional information. So, the novelty of this work lies more in the new opportunities for P-wave velocity estimation than in the specific method we used.

Following the approach of paper 1 and synthetic tests performed by Socco et al. (2016), we used the apparent Poisson's ratio estimated for one reference model to estimate the V_{Pz} along a line where several DCs are available. This means that we assumed that the apparent Poisson's ratio profile has negligible variations along the line. This hypothesis has been motivated in the "Introduction" section and is quite consistent in shallow sedimentary environments where vertical variability of Poisson's ratio is mainly due to water table and/or bedrock top whereas lateral variability is mainly related to changes in the solid matrix properties. As already pointed out in paper 1, the extension to 2D using a single reference model for estimating the W/D relationship and the apparent Poisson's ratio should be checked by analyzing the variability of the DCs within the data set. In our experience, if significant lateral variations exist along the line, they will be evident in the DCs. As an example, we refer to Konstantaki et al. (2013), in which a set of DCs is estimated from seismic data crossing a shallow fault. The DC trend clearly evidenced two different regions at the two sides of the faults, similarly to what happens for field case 2 in this paper.

Because for the two field cases we had independent V_S models, from laterally constrained inversions of the DCs, and V_P models, from the P-wave traveltime tomographies, we have used these results to compute the 2D apparent Poisson's ratio along the survey lines. We compare these 2D apparent Poisson's ratios from independent results with the one estimated with our method for the reference models in Figure 9. We also report in Figure 9 the apparent Poisson's ratio profiles from the DHTs. The two field data sets are characterized by two different conditions in terms of lateral variations. In field case 1, Poisson's ratio does not present significant lateral variations and the estimate of one Poisson's ratio profile can be enough to provide a sufficiently accurate estimate of V_{Pz}. In the second field data set, the geologic setting originates two different zones with different kinds of sediments and water table depths and hence different characteristic Poisson's ratio profiles. These two different zones are clearly evident in the DC data set that presents two well-identified trends (see Figure 10, paper 1). This suggests to use two reference models and to estimate two W/D relationships. In both field cases, our estimated apparent Poisson's ratio compares well with the independent data (Figure 9); in the first meters of the zone north of field case 2, our Poisson's ratio profile shows a greater contrast with respect to the 2D benchmark, but this trend is in better agreement with DHTs than the 2D benchmark. Another significant difference with respect to DHT results is in the first 10 m in the south zone of field case 2, in

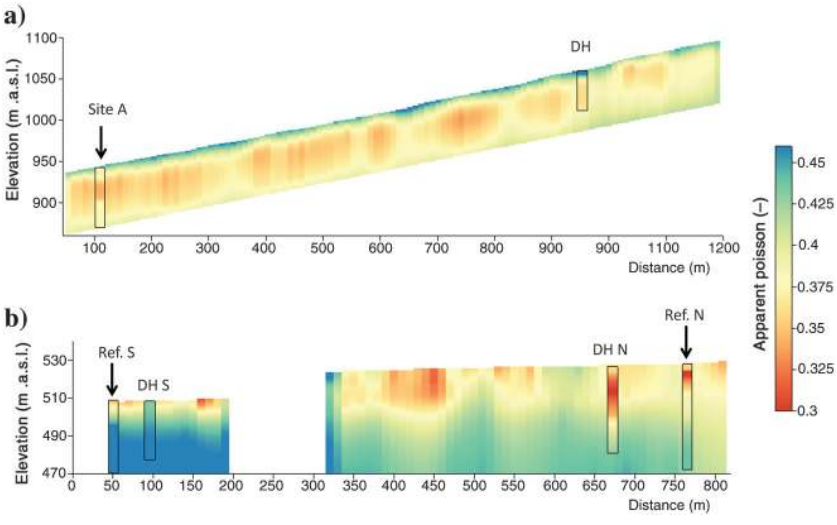

Figure 9. Apparent Poisson's ratio for the two field data sets, field case 1 in (a) and field case 2 in (b), obtained from DC inversion and P-wave tomography compared with Poisson's ratio estimated at the reference models and with Poisson's ratio from DHT tests.

which the DHT shows very high values of Poisson's ratio up to the ground surface whereas both our estimates and the 2D benchmark show a lower value. Nevertheless, this difference is fully due to water table level variations. In fact, DHT was acquired in the spring (during the melting period) whereas the seismic line was acquired in the winter (during the dry period). The expected variability of water table level in the south zone is of several meters, contrary to what observed in the north zone where there is very limited seasonal change.

In the two presented field cases, the reference V_S models were estimated with no bias on Poisson's ratio. In field case 1, the inversion of the DC used to estimate the reference V_S was performed through a Monte Carlo inversion algorithm in which the Poisson's ratio was set free to vary in a wide range (0.2–0.49). In field case 2, the V_S reference model was estimated through the joint inversion of DC and P-wave traveltimes with no constraints on the values of the Poisson's ratio of the initial model. This is very important because if the reference model is obtained through the inversion of a DC using a priori fixed Poisson's ratio value, this will affect the estimate performed using the W/D relationship.

It is important to stress that the proposed approach consists in a data transform: The knowledge of one V_S model along the line is used to estimate the W/D relationship that represents the function for data transform from DC into V_{Sz}. The W/D relationship is then used to estimate the apparent Poisson's ratio that represents the function for the data transform from V_{Sz} into V_{Pz}. Hence, the method is completely data driven and this also affects the final uncertainties. The uncertainties of the estimated V_{Sz} model have been extensively discussed in paper 1. Here, we focus on the uncertainties on V_{Pz}, which are a function of the uncertainty on V_{Sz} and those on the apparent Poisson's ratio. The two field cases have clearly shown a dependency of the result quality to the data quality and coverage. However, in spite of all the approximations involved in the method, the final V_{Pz} sections appear to be a good estimation when compared with the benchmark obtained through P-wave traveltime tomography. In particular, field case 1 shows a difference within 10% with respect to the benchmark and case 2 shows similar differences in most of the zones with good data coverage. Our results are also in good agreement with the ones of DHTs, and the velocity models and traveltimes directly picked from borehole data tend to be in better agreement with our results than with tomograms. It has also to be noted that the used benchmarks do not represent the ground truth, but these are the result of an inversion process and, hence, are affected by an unknown uncertainty that is not considered here. Consistently with paper 1, however, we also used the P-wave traveltime inversion results as a reference for the computation of one-way time. We have shown (Figures 6d and 8d) that the static shift computed from the velocity models obtained through inversion and those obtained from the direct estimation have similar spatial trends and have differences mostly less than 5 ms. Moreover, for field case 2, the comparison of one-way times obtained with our approach with the available DHT traveltimes (Figure 8d) showed that our estimate is in better agreement with the DHT and that both are slightly higher than those obtained from tomography, particularly in the north zone. In Figure 10, we show the difference between the P-wave one-way time for the two sections in Figures 6 and 8. For field case 1, for a floating datum plan at a depth of 55 m, most of the one-way time values (80%) present a difference with a benchmark of less than 2 ms. Hence, they can be considered of the same order of typical time sampling for seismic exploration data. For field case 2, in which the data quality is critical, for a fixed datum plan (at 45 m depth in the north zone and 30 m in the south zone), the difference is greater and the V_{Pz} directly estimated with W/D relationship shows a globally lower value with respect to P-wave traveltime inversion. This reflects in an overestimation of the one-way time. Nevertheless, this overestimation is partly a consequence of the overestimation of V_{Sz} shown in paper 1, and our results are supported by DHT data.

It is important to stress that the two field data sets were acquired for high-resolution shallow seismic investigations. Light sources and dense spatial sampling were used in both cases. This produced high-frequency data that resulted in short wavelengths compared with data normally acquired in hydrocarbon exploration. This limited the investigation depth to few tents of meters, and in neither of the two cases the seismic models have reached the bedrock top. In the synthetic examples, we have shown that the estimation improves with depth, and this makes the results even more promising in the case of greater investigation depth than the one reached here.

This new method is a very fast, even though approximated, way to directly estimate V_P statics from SW dispersion data. As for the direct estimate of V_S statics proposed in paper 1, inversion is not needed and only a local 1D V_S reference model is required for the processing after the DCs are extracted from the data.

As stated in paper 1, because the analysis is performed on local 1D models, there is no difference in applying this method to 2D or 3D data set. The lateral resolution and investigation depth depend on the way DCs have been estimated and on the frequency band of the propagating wavefield. For optimal data processing and requirements on acquisition parameters, one can refer to Socco et al. (2010).

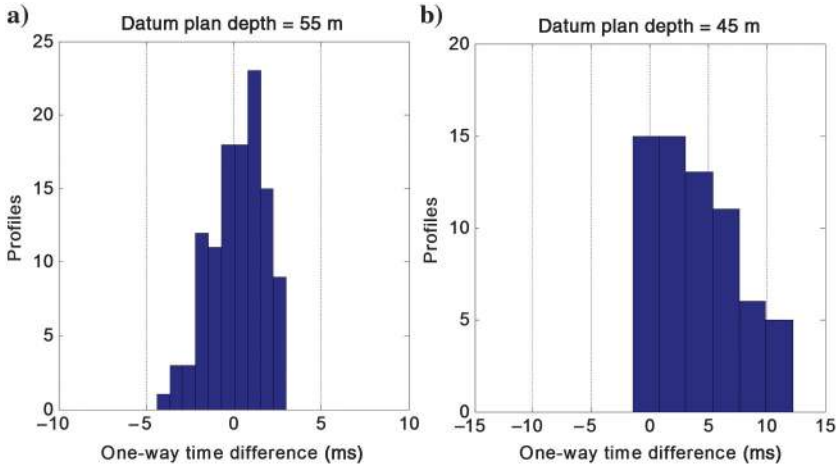

Figure 10. Distribution of the difference in P-wave one-way time between the P-wave traveltime tomography and the direct estimation using our method for (a) field cases 1 and (b) 2. The computation has been performed at every 10 m along the interpolated 2D sections in Figures 6 and 8.

CONCLUSIONS

We have extended the work presented in paper 1 to the direct estimation of P-wave time-average velocity. We have shown that the relationship between SW DC wavelength and the time-average V_S model depth, introduced in paper 1, is sensitive to Poisson's ratio. We have shown that this sensitivity increases with depth, and it can be used to estimate Poisson's ratio for models with constant and variable Poisson's ratio with depth.

For a constant Poisson's ratio with depth, the estimate provides the exact value. For a variable Poisson's ratio, we have introduced the concept of the apparent Poisson's ratio that relates V_{Sz} and V_{Pz}, and we have applied it to the transformation of the V_{Sz} estimated in paper 1 into V_{Pz}. We obtained synthetic and field data results with V_{Pz} uncertainty within 10% for good quality data. When lateral variations are depicted through the analysis of DC trends, we recommend to split the data set into subdata sets and to extract more than one W/D relationship and Poisson's ratio estimation.

The method proposed in this paper, integrated with that proposed in paper 1 for the estimation of V_{Sz}, represents a double data transformation that allows S- and P-wave statics at a datum plan to be estimated from SW DC with no need for inversion, within the investigation depth of SWs. Being a data transformation, the results of this method are fully data dependent. The investigation depth depends on the retrieved wavelength of SW data and Poisson's ratio. This represents the main limitation of the proposed method.

A possible further development of this work is the inversion of the W/D relationship to estimate Poisson's ratio of the layered system with greater accuracy. Nevertheless, we think that if the task is the estimation of P-wave statics, the uncertainty obtained with the simple interpolation proposed here is low enough and that if the data quality is poor, inversion of W/D relationship will suffer from strong nonuniqueness.

Besides the computation of statics, this approach to estimate an approximated V_P model from SW DCs also offers interesting possible developments for other processing needs, such as defining initial models for full-waveform inversions or complementing deep velocity models for any processing applications requiring accurate velocity starting models.

ACKNOWLEDGMENTS

The Seismic Service of the Environment Regional Agency of the Piemonte Region (ARPA Piemonte) and the Natural Risk Management and Observational Seismology Department of the Aosta Valley Region supported the data acquisition and allowed publication of the data of the two field examples. The EU-financed Interreg III B — Alpinespace — Sismovalp project "Seismic hazard and alpine valley response analysis" through which the field data were acquired. We thank P.I. Pecholcs and two anonymous reviewers for their thorough reviews and constructive comments.

REFERENCES

Al Dulaijan, K., and R. R. Stewart, 2010, Using surface-wave methods for static corrections: A near-surface study at Spring Coulee, Alberta: 80th Annual International Meeting, SEG, Expanded Abstracts, 1897–1901.

Bachrach, R., J. Dvorkin, and A. Nur, 2000, Seismic velocities and Poisson's ratio of shallow unconsolidated sands: Geophysics, **65**, 559–564, doi: 10.1190/1.1444751.

Badji, R., M. Speziali, A. Agoudjil, M. Clementi, M. Mantovani, C. Belguermi, M. Benzaoui, S. Bettioui, and A. Hamdani, 2016, Simultaneous joint inversion for near surface characterization — Improving from first break picking to statics: 78th Annual International Conference and Exhibition, EAGE, Extended Abstracts, We SBT4 03, doi: 10.3997/2214-4609.201601151.

Barreto, Y.R., 2013, Surface wave analysis for building near surface velocity models: The role of higher modes: M.S. dissertation, Politecnico di Torino.

Bergamo, P., and L. V. Socco, 2016, P- and S-wave velocity models of shallow dry sand formations from surface wave multimodal inversion: Geophysics, **81**, no. 4, R197–R209, doi: 10.1190/geo2015-0542.1.

Boiero, D., and L. V. Socco, 2014, Joint inversion of Rayleigh-wave dispersion and P-wave refraction data for laterally varying layered models: Geophysics, **79**, no. 4, EN49–EN59, doi: 10.1190/geo2013-0212.1.

Boiero, D., M. Maraschini, and L. V. Socco, 2009, P and S wave velocity model retrieved by multi modal surface wave analysis: 71st Annual International Conference and Exhibition, EAGE, Extended Abstracts, T010.

Boiero, D., P. Marsden, V. Esaulov, A. Zarkhidze, and P. Vermeer, 2013, Building a near-surface velocity model in the South Ghadames Basin: Surface-wave inversion to solve complex statics: 83rd Annual International Meeting, SEG, Expanded Abstracts, 1811–1815.

Boore, D., 2007, Dave Boore's notes on Poisson's ratio (the relation between V_P and V_S), http://www.daveboore.com/daves_notes.html, accessed 03 March 2017.

Dunkin, J, 1965, Computation of modal solutions in layered, elastic media at high frequencies: Bulletin of Seismological Society of America, **55**, 335–358.

Ernst, F., 2008, Multi-mode inversion for P-wave velocity and thick near-surface layers: 14th European Meeting of Environmental and Engineering Geophysics, EAGE, Extended Abstracts, A13, doi: 10.3997/2214-4609.20146236.

Foti, S., and C. Strobbia, 2002, Some notes on model parameters for surface wave data inversion: Symposium on the Application of Geophysics to Engineering and Environmental Problems SAGEEP, SEI6, doi: 10.4133/1.2927179.

Gendrin, A., E. Muyzert, M. Williams, I. Bradford, I. Rodriguez, and A. Probert, 2015, Impact of near-surface velocities on surface microseismic signal — A case study in the Fayetteville formation: 77th Annual International Conference and Exhibition, EAGE, Extended Abstracts, We N116 11.

Haskell, N., 1953, The dispersion of surface waves on multilayered media: Bulletin of the Seismological Society of America, **43**, 17–34.

Herrmann, R. B., and C. J. Ammon. 2002, Computer program in seismology — Surface waves, receiver functions and crustal structure, version 3.20: Saint Louis University, MO 110 p.

Karray, M., and G. Lefebvre, 2008, Significance and evaluation of Poisson's ratio: Canadian Geotechnical Journal, **45**, 624–635, doi: 10.1139/T08-016.

Konstantaki, L. A., S. Carpentier, F. Garofalo, P. Bergamo, and L. V. Socco, 2013, Determining hydrological and soil mechanical parameters from multichannel surface wave analysis across the alpine fault at inchbonnie, New Zealand: Near Surface Geophysics, **11**, 435–448, doi: 10.3997/1873-0604.2013019.

Maraschini, M, 2008, A new approach for the inversion of Rayleigh and Scholte waves in site characterization: Ph.D. dissertation, Politecnico di Torino.

Nazarian, S., 1984, In situ determination of elastic moduli of soil deposits and pavement systems by spectral-analysis-of-surface waves method: Ph. D. dissertation, The University of Texas at Austin.

Pan, Y., J. Xia, L. Gaoa, C. Shen, and C. Zeng, 2013, Calculation of Rayleigh-wave phase velocities due to models with a high-velocity surface layer: Journal of Applied Geophysics, **96**, 1–6, doi: 10.1016/j.jappgeo.2013.06.005.

Pelekis, P. C., and G. A. Athanasopoulos, 2011, An overview of surface wave methods and a reliability study of a simplified inversion technique: Soil Dynamics and Earthquake Engineering, **31**, 1654–1668, doi: 10.1016/j.soildyn.2011.06.012.

Ponomarenko, A., B. Kashtan, V Troyan, and W. Mulder, 2013, Surface wave inversion for a P-wave velocity profile via estimation of the squared slowness gradient: 75th Annual International Conference and Exhibition, EAGE, Extended Abstracts, doi: 10.3997/2214-4609.20130945.

Socco, L. V., C. Comina, and F. Khosro Anjom, 2017, Direct static estimation through surface wave analysis: Part 1 — S-wave velocity: Geophysics, **82**, this issue, doi: 10.1190/geo2016-0367.1.

Socco, L. V., C. Comina, F. Khosro Anjom, and T. O. Akintola, 2016, P- and S-wave direct static estimation from surface wave dispersion data: 78th Annual International Conference and Exhibition, EAGE, Extended Abstracts, We SBT4 02.

Socco, L. V., and D. Boiero, 2008, Improved Monte Carlo inversion of surface wave data: Geophysical Prospecting, **56**, 357–371, doi: 10.1111/j.1365-2478.2007.00678.x.

Socco, L. V., D. Boiero, C. Comina, S. Foti, and R. Wisén, 2008, Seismic characterization of an alpine site: Near Surface Geophysics, **6**, 255–267, doi: 10.3997/1873-0604.2008020.

Socco, L. V., D. Boiero, S. Foti, and R. Wisén, 2009, Laterally constrained inversion of ground roll from seismic reflection records: Geophysics, **74**, no. 6, G35–G45, doi: 10.1190/1.3223636.

Socco, L. V., S. Foti, and D. Boiero, 2010, Surface wave analysis for building near surface velocity models: established approaches and new perspectives: Geophysics, **75**, no. 5, 75A83–75A102, doi: 10.1190/1.3479491.

Strobbia, C., A. El Emam, J. Al-Genai, and J. Roth, 2010, Rayleigh wave inversion for the near-surface characterization of shallow targets in a heavy oil field in Kuwait: First Break, **28**, 103–109.

Thomson, W., 1950, Transmission of elastic waves through a stratified solid medium: Journal of Applied Physics, **21**, 89–93, doi: 10.1063/1.1699629.

van Dedem, E. J., F. Ernst, and J. Shorter, 2014, Deriving P-wave near-surface models from exploration data: 76th Annual International Conference and Exhibition, EAGE, Extended Abstracts, WS6–C04.

Xia, J., R. D. Miller, and C. B. Park, 1999, Estimation of near-surface shear-wave velocity by inversion of Rayleigh wave: Geophysics, **64**, 691–700, doi: 10.1190/1.1444578.

Xia, J., R. D. Miller, C. B. Park, and G. Tian, 2003, Inversion of high frequency surface waves with fundamental and higher modes: Journal of Applied Geophysics, **52**, 45–57, doi: 10.1016/S0926-9851(02)00239-2.

Zimmer, M. A., M. Prasad, G. Mavko, and A. Nur, 2007, Seismic velocities of unconsolidated sands: Part 1 — Pressure trends from 0.1 to 20 MPa: Geophysics, **72**, no. 1, E1–E13, doi: 10.1190/1.2399459.